Invited paper

MEMS reliability assessment: preliminary results

Donald R. Skelton[1], **James L. Zunino III**[1], **Wei Han**[2], and **Ryszard J. Pryputniewicz**[2]

[1]U.S. Army RDE Command, Attn: AMSRD-AAR-AEE-P
Energetics, Warheads & Environmental Tech. U.S. Army Corrosion Office
Metallic Materials Technology Branch, Bldg 60
Picatinny Arsenal, NJ 07806-5000
Phone: (973) 724-6773 Fax (973) 724-4525
Email:donald.skelton@us.army.mil; james.zunino@us.army.mil

[2] WPI-ME/CHSLT-NEST, Worcester, MA 01609, Email: rjp@wpi.edu

ABSTRACT

The quality and reliability of MEMS are greatly impacted by compatibility of materials used in a package. Inadequate understanding of MEMS reliability adversely affects their utilization, especially those requiring "long-term storage". Current trend in micro/nanosystems is to produce ever smaller, lighter, and more capable devices/sensors in greater quantities and at a lower cost than ever before. In addition, the finished products have to operate at very low power and in very adverse conditions while assuring durable and reliable performance. Performance of MEMS has advanced to the point that package induced stresses now limit further improvements in accuracy and stability. Optimization of a MEMS package for high performance is limited by these constraints and cannot be accomplished by analysis alone. There are too many unknown material properties, process conditions, and assembly tolerances to make this feasible. This paper describes the methodology and discusses preliminary results that have been obtained relating measurements that facilitate MEMS reliability assessment (MRA) on representative samples used. Regardless of their application, the MEMS have to be reliable while in use. MEMS reliability, however, is application specific and, usually, has to be developed on a case by case basis. The results presented herein were obtained, using a recently developed optoelectronic laser interferometric microscope (OELIM) methodology, in a planned program on **MEMS reliability assessment**. The presentation is illustrated with selected examples representing the OELIM study of specific MEMS. By quantitatively determining performance of MEMS, under different operating conditions, we can develop a better understanding of their operational characteristics, which will ensure that they are operated at optimum conditions, are durable, and are reliable.

Keywords: MEMS, OELIM methodology, reliability assessment, thermal, static, and dynamic loads.

1. INTRODUCTION

MEMS is a revolutionary enabling technology (ET) [1,2]. It defines both the methodologies to make these systems and the systems themselves [3]. This technology merges the functions of sensing, actuation, and controls with computation and communication to affect the way that people and machines interact with the physical world. This is done by integrating advances in various multidisciplinary fields to produce very small devices that use very low power and operate in many different environments [4]. Today, developments in MEMS are being made at an unprecedented rate, driven by (both) technology and user requirements.

Effective development of MEMS, however, requires knowledge of design, analysis/simulation, materials, fabrication, with special emphasis on innovative packaging, and testing/characterization of the finished products [1]. As such,

effective development of MEMS requires special processes, e.g., multilevel sacrificial surface micromachining (SSM), and rigorous education of practitioners of ET to use these processes.

A unique technology, recently developed at Sandia National Laboratories (SNL), is the only process technology that allows up to five independent structural levels for construction of MEMS [5], permitting development of complex systems with micron feature sizes [6]; other processes use (typically) up to three structural levels. The Sandia's Ultraplanar MEMS Multi-level Technology (SUMMiT™) consists of an integrated set of design and layout tools, including visualization and checking of design rules, for use with the 5-level SUMMiT™ fabrication, as well as post-fabrication release, packaging, reliability characterization, and failure analysis [5]. Worcester Polytechnic Institute (WPI) has formed an alliance with SNL to teach this new technology [7]. As a result, a number of courses were developed as a part of NEST (NanoEngineering, Science, and Technology) Program at WPI [4,8]. These courses, each one semester long, are offered at the graduate/advanced-undergraduate levels.

The first course introduces students to the field of MEMS, including design, analysis, and fabrication, based on multilevel SSM, emphasizing integration of nanotechnology with MEMS [4]. Bulk and thin film properties of materials, used for fabrication of MEMS, are discussed [9]. This leads to detailed discussions of the SUMMiT™ V process, featuring fabrication concepts, process design, layout, and visualization tools; the discussions are supported by active use of the SUMMiT™ V software. Class projects give students an opportunity to design their own MEMS using the SUMMiT™ V software tools, perform analyses using finite element method (FEM) software packages [10-12], and prepare documentation of their designs for fabrication at SNL.

The second course addresses release, testing, packaging, as well as reliability and failure analysis of MEMS; students work on these issues in a project mode, in groups of two or more. Testing and analysis determines electrical and mechanical characteristics of MEMS, using commercial electronic instrumentation and in-house developed *optoelectronic laser interferometric microscope* (OELIM) methodology [3], respectively. Measured results are correlated with the results of analysis, subject to uncertainty considerations [13]. The projects are rigorously documented in detailed reports, which are required, in addition to homework and exams.

Because of the nature of topics covered, both courses are based on an integrated use of analytical, computational, and experimental solutions (ACES) methodology [14], which we find particularly suitable for the development of MEMS [9,15]. In the ACES methodology, the analytical results are obtained using exact closed form solutions, the computational results are either based on the FEM, or the boundary element method (BEM), or the finite difference method (FDM) solutions, while the experimental results rely on the OELIM solutions.

Recent advances in microtechnology allow monolithic integration of MEMS with driving, controlling, and signal processing electronics [16]. This integration improves performance of micromechanical devices as well as reduces the cost of fabricating, packaging, and interconnecting these devices by combining them with an electronic subsystem in the same fabrication and packaging process [17]. Using SUMMiT™ V process enables fabrication of complex mechanical systems with intricate coupling mechanisms [18]. These systems are batch fabricated, with no piece part assembly required, ready to use at the end of the fabrication process [6]. In this paper we describe use of the *optoelectronic methodology* which is used for measurements that facilitate MEMS reliability assessment (MRA) [19-21].

2. REPRESENTATIVE MEMS SAMPLES USED

Following representative MEMS samples are used in this paper: 1) microgyroscope, and 2) cantilever-type Ohmic-contact for a microswitch.

In the configuration shown in Fig. 1, used in this study, a microgyroscope is actuated by electrostatic comb drives. The comb drives, in turn, are excited in such a way that the electrostatic forces they generate depend on lateral position(s) of the proof masses (i.e., shuttles). The resulting (large) amplitude vibrations/oscillations, parallel to teeth of the comb drives, increase sensitivity of a microgyro and reduce errors from external forces. Angular rate, with respect to the axis located in the plane of the shuttles, lifts one mass up and lowers the other mass down due to the Coriolis forces. Capacitors, usually located below the shuttles, sense these up and/or down motions. The shuttles are mounted/attached to the substrate through suspension springs, Fig. 2. The mode of operation where the shuttles move in opposite directions lowers sensitivity of a microgyro to linear acceleration. The two vibrating shuttles, suspended by folded springs, are driven by electrostatic comb drives to maintain lateral in-plane oscillation.

The microswitch considered in this study is a cantilever-type radio frequency (RF) MEMS switch [22], Fig. 3. Voltage applied to the electrodes induces an electrostatic force that activates/actuates the microswitch [23] . An electrostatic force bends the cantilever causing its contacts to touch (i.e., by reducing the gap distance, d_g, to zero), which closes an electrical path (by making a cross-bar to close the "opening" in a trace below the free end of a microcantilever) and facilitates propagation of a signal. As the activation/actuation voltage is released, elasticity of the microcantilever is used to return it to its original, or open, position (i.e., making d_g>0).

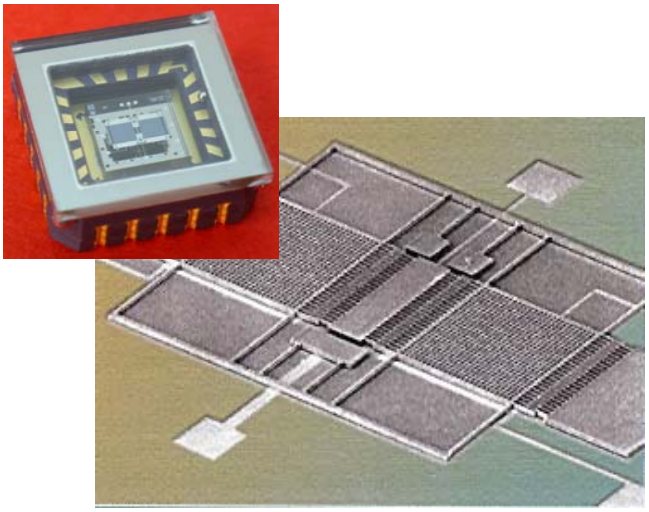

Fig. 1. Typical microgyro package (top left) and a representative inertial MEMS sensor (in the background).

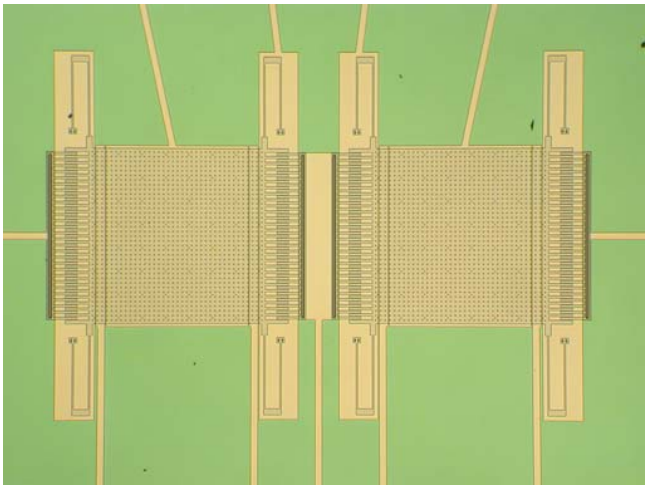

Fig. 2. Close-up of the shuttles and folded suspension springs, one spring is used in each of 4 corners of a shuttle.

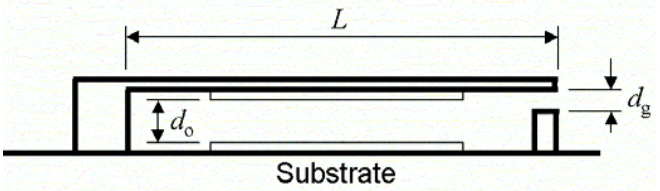

Fig. 3. RF MEMS switch: microcantilever configuration, electrical traces were omitted for simplicity.

Mechanically, a microcantilever of a switch behaves like a conventional cantilever [23]. In fact, traditional equations can be used to find microcantilever stiffness, natural frequency, pull-in voltage, and magnitude of the activation/actuation force [4]. The switch fabrication methods are particularly important because they dictate the material type, surface finish, texture, and overall size of the microswitch components (especially, its electrical interfaces). Consequently, material properties have a direct influence on performance characteristics of a microswitch and its behavior under actual operating conditions [24]. In fact, fabrication tolerances and accuracy of material properties have profound influence on dynamics as well as the performance of microswitches [22,25].

3. SOLUTIONS USED

Effective and efficient *MEMS reliability assessment* can be achieved using a combination of analytical, computational, and experimental solutions (ACES) [26,27].

3.1. Analytical solution

An initial goal of analysis of a microgyroscope, and/or any other MEMS is (usually) to determine accelerations of all moving parts of a device. Then, using Newton's Second Law, forces acting on the MEMS are calculated [28,29].

Once the dynamic forces are known, we can determine whether the microdevices will perform as anticipated under expected operating conditions, or not.

Dynamic forces are based on accelerations, both linear and angular. In order to calculate accelerations we must first determine positions of all components in a microsystem for each increment of the input motion, i.e., as a function of time into a cycle of operation [29]. Once equations defining positions are known, we differentiate them with respect to time to calculate velocities, and then differentiate again to obtain accelerations.

3.2. Computational solution

Computational modeling of MEMS can be performed using commercial software tools [10,11,30,31] . Parametric templates, utilizing, e.g., Python scripting, for modeling MEMS can be developed and utilized for in-depth understanding of the designed/expected operation of microsystems. MEMS geometry, material properties, stress, contact forces, dynamic response, and other parameters can be investigated using the parametric templates to optimize performance. Atmospheric conditions (including vacuum), geometry of MEMS, as well as optimized pull-down voltage profiles can be modeled to understand and optimize dynamic damping conditions of a packaged or unpackaged MEMS [32].

Coupled electrostatics-structure-flow simulations can also be performed using CFD-ACE+ software because it has the necessary multiphysics capabilities including flow, heat-transfer, mechanics, and electrostatics [30]. All CFD-ACE+ capabilities are fully coupled for fast and accurate results. For this study, linking between electrostatics, structural mechanics, and flow was of interest.

3.3. Experimental solution

The experimental solution in this paper was obtained using *optoelectronic methodology*, which is based on the principles of *optoelectronic holography* (OEH) [3,33,34]. Basic configuration of the OEH system is shown in Fig. 4. In this configuration, laser light is launched into a single mode optical fiber by means of a microscope objective (MO). Then, the single mode fiber is coupled into two fibers by means of a fiber optic directional coupler (DC). One of the optical fibers comprising the DC is used to illuminate the object, while the output from the other fiber provides reference against which the signals from the object are recorded. Both, the object and the reference beams are combined by the interferometer (IT) and recorded by the system camera (CCD).

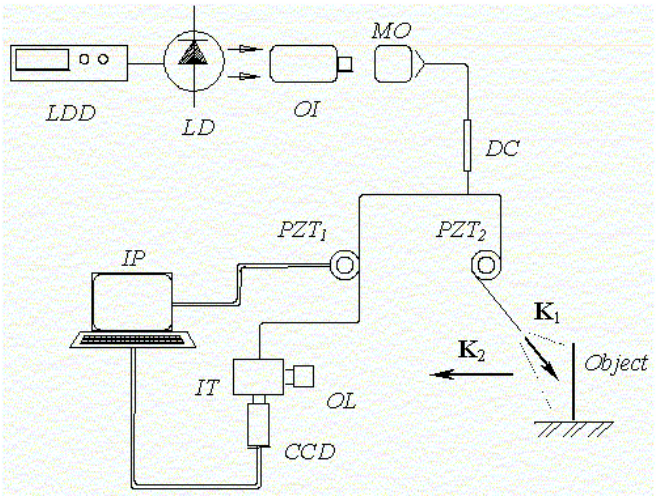

Fig. 4. Single-illumination and single-observation geometry of a fiber optic based OEH system: *LDD* is the laser diode driver, *LD* is the laser diode, *OI* is the optical isolator, *MO* is the microscope objective, *DC* is the fiber optic directional coupler, PZT_1 and PZT_2 are the piezoelectric fiber optic modulators, *IP* is the image-processing computer, *IT* is the interferometer, *OL* is the objective lens, *CCD* is the camera, while $\mathbf{K}_1$ and $\mathbf{K}_2$ are the directions of illumination and observation, respectively.

Images recorded by the CCD are processed by the image-processing computer (IP) to determine the fringe-locus function, $\Omega(x,y)$, constant values of which define fringe loci on the surface of an object being investigated. The values of Ω relate to the system geometry and the unknown vector $\mathbf{L}(x,y)$**,** defining displacements/deformations, via the relationship [35]

$$\Omega(\mathbf{x},\mathbf{y}) = \mathbf{K}(\mathbf{x},\mathbf{y}) \bullet \mathbf{L}(\mathbf{x},\mathbf{y}) = (\mathbf{K}_2 - \mathbf{K}_1) \bullet \mathbf{L} \quad , \tag{1}$$

where $\mathbf{K}(x,y)$ is the sensitivity vector defined in terms of vectors $\mathbf{K}_1$ and $\mathbf{K}_2$ identifying directions of illumination and observation, respectively, in the OEH system, Fig. 4.

Quantitative determination of structural displacements and deformations due to the applied loads can be obtained, by solving a system of equations similar to Eq. 1, to yield [35]

$$\mathbf{L} = \left[\tilde{\mathbf{K}}^{\mathrm{T}} \tilde{\mathbf{K}}\right]^{-1} \left(\tilde{\mathbf{K}}^{\mathrm{T}} \Omega\right) \quad , \tag{2}$$

where $\tilde{\mathbf{K}}^{\mathrm{T}}$ represents the transpose of the matrix of the sensitivity vectors **K**. Equation 2 indicates that displacements/deformations determined from interferograms are functions of **K** and Ω, which have spatial, i.e., (x,y), distributions over the field of interest on an object being investigated. In addition, Eq. 2 can be represented by a phenomenological relation [13]

$$\mathbf{L} = \mathbf{L}(\mathbf{K}, \Omega) \quad , \tag{3}$$

based on which the RSS-type (where RSS represents *the square Root of the Sum of the Squares*) uncertainty in **L**, i.e., $\delta\mathbf{L}$, can be determined to be

$$\delta\mathbf{L} = \left[\left(\frac{\partial \mathbf{L}}{\partial \mathbf{K}} \delta\mathbf{K} \right)^2 + \left(\frac{\partial \mathbf{L}}{\partial \Omega} \delta\Omega \right)^2 \right]^{1/2} \quad , \tag{4}$$

where $\partial\mathbf{L}/\partial\mathbf{K}$ and $\partial\mathbf{L}/\partial\Omega$ represent partial derivatives of **L** with respect to **K** and Ω, respectively, while $\delta\mathbf{K}$ and $\delta\Omega$ represent the corresponding uncertainties in **K** and Ω, respectively. It should be remembered that **K**, **L**, and Ω are all functions of spatial coordinates (x,y,z), i.e., $\mathbf{K} = \mathbf{K}(x,y,z)$, $\mathbf{L} = \mathbf{L}(x,y,z)$, and $\mathbf{\Omega} = \mathbf{\Omega}(x,y,z)$, respectively, when performing partial differentiations. After evaluating, Eq. 4 indicates that $\delta\mathbf{L}$ is proportional to the product of the local value of **L** with the RSS value of the ratios of the uncertainties in **K** and Ω to their corresponding local values, i.e.,

$$\delta\mathbf{L} \propto \mathbf{L} \left[\left(\frac{\delta\mathbf{K}}{\mathbf{K}} \right)^2 + \left(\frac{\delta\Omega}{\Omega} \right)^2 \right]^{1/2} \quad . \tag{5}$$

For typical geometries of the OEH systems used in recording of interferograms, the values of $\delta\mathbf{K}/\mathbf{K}$ are less than 0.01. However, for small deformations, the typical values of $\delta\Omega/\Omega$ are (usually) more than one order of magnitude greater than the values for $\delta\mathbf{K}/\mathbf{K}$. Therefore, the accuracy with which the *fringe orders* (based on which Ω values are calculated) are determined influences the accuracy in the overall determination of displacements/deformations [36]. To minimize this influence, a number of algorithms for determination of Ω were developed. Some of these algorithms require multiple recordings of each of the two states, in the case of *double-exposure method*, of the object being investigated with introduction of a discrete phase step between the recordings [37,38].

For example, the intensity patterns of the first and the second exposures, $I_n(x,y)$ and $I'_n(x,y)$, respectively, in the *double-exposure sequence*, can be represented by the following equations:

$$I_n(x,y) = I_o(x,y) + I_r(x,y) + 2\left\{\left[I_o(x,y)\right]\left[I_r(x,y)\right]\right\}^{1/2} \cos\left\{\left[\Delta\varphi(x,y)\right] + \theta_n\right\} \tag{6}$$

and

$$I'_n(x,y) = I_o(x,y) + I_r(x,y) + 2\left\{\left[I_o(x,y)\right]\left[I_r(x,y)\right]\right\}^{1/2} \cos\left\{\left[\Delta\varphi(x,y)\right] + \theta_n + \Omega(x,y)\right\} \quad , \tag{7}$$

where $I_o(x,y)$ and $I_r(x,y)$ denote the object and reference beam intensities, respectively, with (x,y) denoting spatial coordinates, $\Delta\varphi(x,y) = \varphi_o(x,y) - \varphi_r(x,y)$ is the optical phase difference based on $\varphi_o(x,y)$, denoting random phase of the light reflected from the object, and $\varphi_r(x,y)$, denoting the phase of the reference beam, θ_n denotes the discrete applied n^{th} phase step, and Ω is the fringe-locus function relating to the displacements/deformations the object incurred

between the first and the second exposures; Ω *is what we need to determine*. When Ω is known, it is used in Eq. 2 to find **L**.

In the case of 5-phase-steps algorithm with $\theta_n = 0, \pi/2, \pi, 3\pi/2, \text{and } 2\pi$, the distribution of the values of Ω can be determined using [33]

$$\Omega(x,y) = \tan^{-1}\left\{\frac{2[I_2(x,y) - I_4(x,y)]}{2I_3(x,y) - I_1(x,y) - I_5(x,y)}\right\} \quad . \tag{8}$$

Results produced by Eq. 8 depend on capabilities of the illumination, the imaging, and the processing subsystems of the OEH system used. Developments in laser, fiber optic, CCD camera, and computer technologies have led to advances in the OEH metrology; in the past, these advances have almost paralleled the advances in the image recording media [39].

In response to the needs of the emerging MEMS technology, an OELIM system for studies of objects with micron size features was developed [34,40,41], Fig. 5.

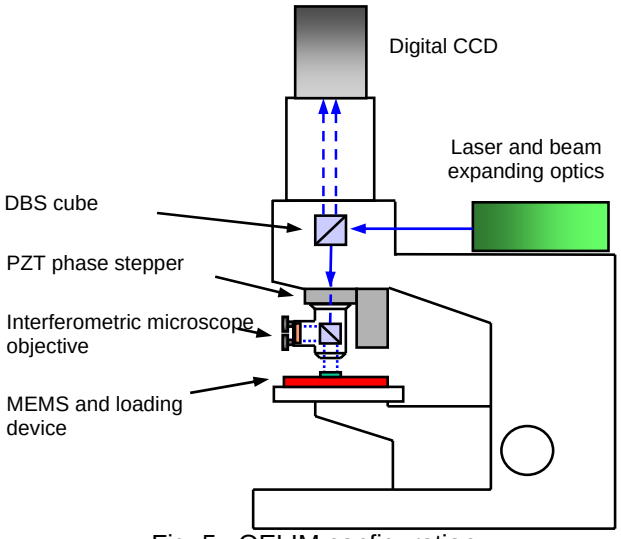

Fig. 5. OELIM configuration.

In the OELIM system, Fig. 5, light beam from a laser is directed into a directional beam splitter (DBS) cube, which produces an *object beam* that is sent into a PZT phase stepper controlled microscope objective. The objective, in turn, illuminates MEMS being investigated; the particular characteristic of the configuration shown is that its specially designed objective has a *long working distance* providing ample space for installation of an *environmental chamber* and/or other *loading device(s)*, as needed.

It should be noted that in the implementation of the OELIM system used in this study, the environmental chamber permitted simultaneous control of pressure/vacuum, temperature (heating and cooling), as well as dynamic excitation (needed for vibrations) of the test samples being characterized/developed.

The object beam reflected by MEMS passes back through the objective to the DBS where it is combined with a *reference beam*. The two beams, recombined at the DBS, are imaged onto the sensing element of a CCD camera, which records intensity distributions of the resulting *interference patterns*. These patterns are transferred to the system computer for subsequent quantitative processing to determine $\Omega(x,y)$ according to Eq. 8.

4. REPRESENTATIVE RESULTS

The *optoelectronic methodology* described in the foregoing discussion was used to determine displacements and deformations of the MEMS samples described in the Section 2. Results of these determinations are summarized in Sections 4.1 and 4.2, respectively.

4.1. Deformations of a microgyroscope

Deformations of proof masses/shuttles were measured during operation of a microgyroscope. In this application, interferograms were recorded stroboscopically while microgyros were driven at their operating frequencies. To facilitate these recordings, the optoelectronic system was set up to be sensitive to the out-of-plane motions. Representative interferograms, corresponding to deformations of the left shuttle of a microgyro operating at 10.1 kHz, are shown in Fig. 6. Observation of the fringe patterns of Fig. 6 clearly indicates asymmetry in deformations of the proof mass(es) of a microgyroscope. This can be related to structural design and suspension of the shuttles as well as to the way that electrostatic forces affect their motions and deformations. A representative display of deformations of the left shuttle of a microgyro operating at 10.1 kHz, during a specific instant in a vibration cycle, is given in Fig. 7, indicating deformations ranging up to 212 nm, which ideally should not exist. However, the deformations/motions were measured, in this case, to be orders of magnitude greater than typical (magnitudes of) motions of the proof masses due to the Coriolis forces.

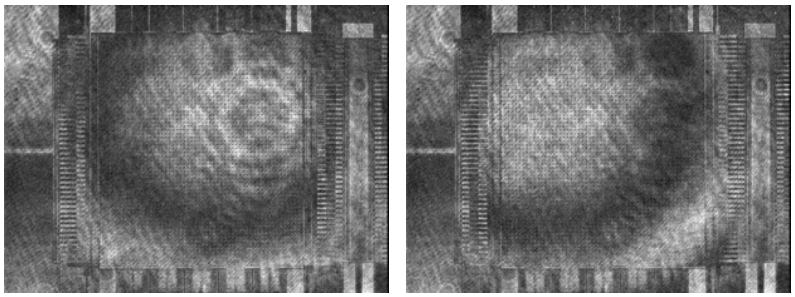

Fig. 6. Representative OELIM fringe patterns of the left shuttle, at different times in a vibration cycle, while a microgyro is operating at 10.1 kHz.

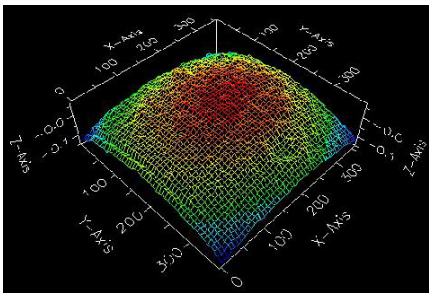

Fig. 7. The out-of-plane 212 nm deformation component of the left shuttle, based on Fig. 6.

Accuracy and precision of a microgyro depends on the quality of its suspension. This suspension is provided by folded springs attached, at one end, to proof masses/shuttles and, at the other end, to posts forming a part of a substrate, Fig. 2. Any deformations of the springs that are not in response to functional operation of a sensor will cause an incorrect (i.e., erroneous) output. For example, thermomechanical distortions of a package affect shape of posts and these, in turn, lead to undesired deformations of the springs and erroneous results produced by a sensor supported by these springs [38,42]. Because of the nanoscale of these deformations and microsize objects over which they take place, it was not until the advancement of optoelectronic metrology that such deformations were quantified in the full-field-of-view (FFV) indicating that thermomechanical deformations of a post are on the nanometer scale [38].

Figure 8 displays representative deformations of a folded spring supporting the left proof mass of a microgyro, as measured using the OELIM methodology. These deformations are about 300 nm, over the section of the microgyro displayed, i.e., the upper-right spring of the left shuttle, as shown in Fig. 2. More specifically, the folded spring, shown in Fig. 8, deforms approximately 126 nm between the point where it is attached to the post and the point of its attachment to the proof mass [43]. The proof mass itself has the deformation of about 174 nm.

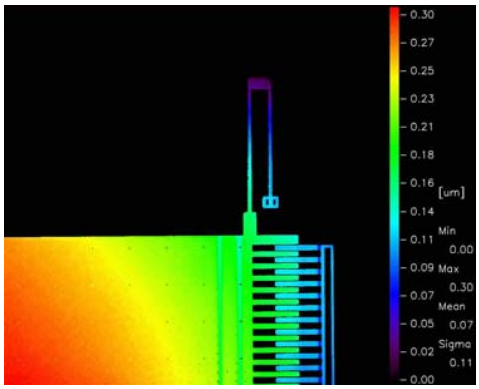

Fig. 8. OELIM measured deformations of the upper right section of the left proof mass of a MEMS gyroscope, Fig. 2, maximum deformation is 300 nm: 2D contour representation.

4.2. Deformations of a cantilever microcontact

MEMS RF switches present a promising technology for high-performance reconfigurable microwave and millimeter wave circuits [44]. Low insertion loss, high isolation, and excellent linearity provided by MEMS switches offer significant improvements over an electrical performance provided by conventional p-i-n diode and metal-oxide semiconductor field-effect transistor (MOSFET) switching technologies. These superior electrical characteristics permit design of MEMS switched high-frequency circuits not feasible with semiconductor switches, such as high-efficiency broadband amplifiers and quasi-optic beam steering arrays. In addition, operational benefits arise from low power consumption, small size and weight, and integration capability of modern RF MEMS switches. Effective computational simulation of a RF MEMS switch must simultaneously combine different loads including, but not limited to, the following: electromagnetic, electrostatic, thermal, mechanical, and aeroelastic [32]. A representative result of such computational multiphysics modeling is shown in Fig. 9, which indicates damping effects of air "surrounding" the microswitch in its package. Figures 10 to 12 illustrate OELIM measured deformations of the same 350 μm long Ohmic-type Si-contact of a microswitch at three different frequencies.

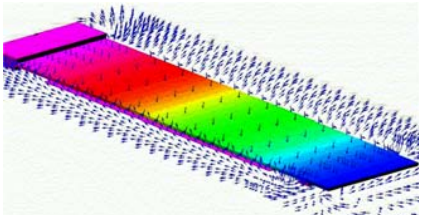

Fig. 9. Computational multiphysics simulation of a RF MEMS contact closure at atmospheric conditions: 3D representation of air damping.

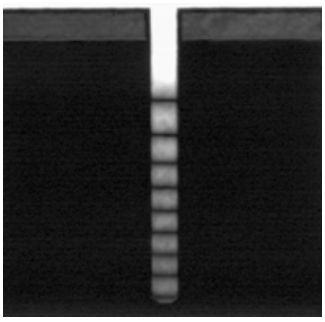

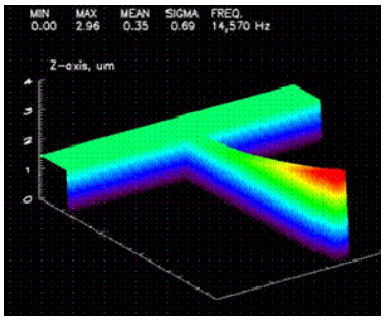

Fig. 10. OELIM measurements of a vibrating MEMS cantilever – resonating at a frequency of 14,570 Hz corresponding to the first flexure mode: (a) time-average fringe pattern, (b) mode shape corresponding to the fringe pattern of part (a).

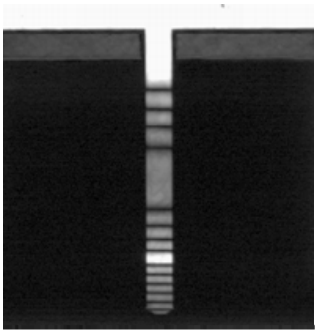

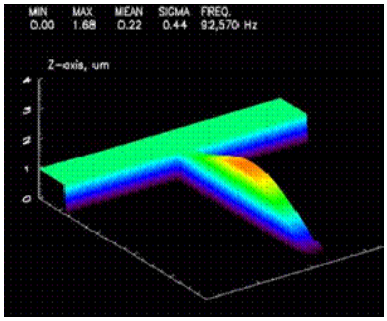

Fig. 11. OELIM measurements of a vibrating MEMS cantilever – resonating at a frequency of 92,570 Hz corresponding to the second flexure mode: (a) time-average fringe pattern, (b) mode shape corresponding to the fringe pattern of part (a).

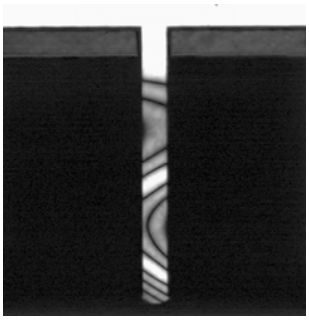

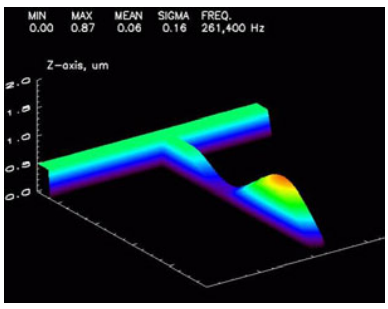

Fig. 12. OELIM measurements of a vibrating MEMS cantilever – resonating at a frequency of 261,400 Hz showing a complex third "flexure" mode: (a) time-average fringe pattern, (b) mode shape corresponding to the fringe pattern of part (a).

In some applications, the damping effects, displayed in Fig. 9, help control switch dynamics and enhance tribological characteristics of the microcontacts; in others, they adversely affect performance of microcontacts [4].

Prototype microcantilevers were fabricated and their dynamic characteristics were determined in real-time using the OELIM methodology. Representative results obtained for a 350 μm long Si microcantilever, Figs 10 to 12, indicate that as the actuation conditions change the corresponding operational response of a microswitch also changes. For example, a microcantilever vibrating at 14,570 Hz has the maximum amplitude of 2.96 μm while the same microcantilever vibrating at 92,570 Hz has the amplitude of 1.68 μm, while the complex mode at 261,400 Hz exhibits amplitude of only 870 nm, all three measured in air at atmospheric pressure to correspond with the conditions used to produce the result displayed in Fig. 9.

Functional operation of microswitches is greatly affected by thermal management (TM) of Joule heat effects generated at the electrical interfaces of these MEMS switches [24]. As a result, careful attention to TM has a profound effect on reliability of microswitches, which are used in virtually every aspect of today's advanced technology.

5. CONCLUSIONS AND FUTURE WORK

An *optoelectronic methodology for development of MEMS* was presented. Suitability of this methodology in experimental mechanics on the micro/nanoscale was demonstrated by applications to representative MEMS. Deformations of the maximum magnitude of 4 nm were measured on MEMS samples that were considered in previous studies.

The methodology is applicable under static and dynamic conditions. In this paper, its applicability was illustrated by use of two representative MEMS samples: microgyroscope, and a cantilever-type Ohmic-microswitch. Deformations of these samples were from a few nm to a few hundred nm, depending on the specific operating conditions and nature of the MEMS considered. Theoretical results correlated with the experimental results, well within the criteria specified by the *uncertainty analysis*. Validated correlations will lead to establishment of "design by analysis" *methodology for efficient and effective MEMS reliability assessment*.

By understanding details of MEMS performance in three-dimensions, we can make specific suggestions for improvements in their design which, in turn, will enhance their operating characteristics. Once the improvements are implemented, we can verify their effectiveness by determining new static and dynamic characteristics corresponding to the improvements made on MEMS.

All in all, the preliminary results presented in this paper indicate that the *optoelectronic methodology* is a viable tool *for MEMS reliability assessment*. In fact, we believe that this methodology may become a *differentiating factor* in developments of *high-performance MEMS* to satisfy ever increasing requirements especially those relating to the *Q-factor* [25] *discrimination*.

6. ACKNOWLEDGMENTS

This paper was supported by the US Army MEMS Reliability Assessment (MRA) Project under Contract No. N65236-06-D-5871. It was also partially supported by the NEST Program at WPI-ME/CHSLT.

7. REFERENCES

1. Pryputniewicz, R. J., "Integrated approach to teaching of design, analysis, and characterization in micromechatronics," *Paper No. IMECE2000/DE-13*, ASME - Am. Soc. Mech. Eng., New York, NY, 2000.
2. Pryputniewicz, R. J., "MEMS design education by case studies," *Paper No. IMECE2001/DE-23292*, ASME - Am. Soc. Mech. Eng., New York, NY, 2001.
3. Pryputniewicz, R. J., and Furlong, C., "Novel optoelectronic methodology for testing of MOEMS," *Proc. Internat. Symp. on MOEMS and Miniaturized Systems III*, SPIE-4983:11-25, 2003.
4. Pryputniewicz, R. J., and Furlong, C., *MEMS and nanotechnology*, Worcester Polytechnic Institute, Worcester, MA, 2002.

5. Shepherd, E., “Prototyping with SUMMiT™ technology, Sandia’s Ultra-planar Multi-level MEMS Technology,” *Paper No. IMECE2002-34258*, Am. Soc. Mech. Eng., New York, NY, 2002.
6. Pryputniewicz, E. J., *Study of design, analysis, fabrication, characterization, and reliability of MEMS at Sandia*, Sandia National Laboratories, Albuquerque, NM, 2000.
7. Pryputniewicz, R. J., Shepherd, E., Allen, J. J., and Furlong, C., “University – National Laboratory alliance for MEMS education,” *Proc. 4th Internat. Symp. on MEMS and Nanotechnology* (*4th-ISMAN*), Charlotte, NC, pp. 364-371, 2003.
8. Pryputniewicz, R. J., *MEMS SUMMiT™ technology*, Worcester Polytechnic Institute, Worcester, MA, 2002.
9. Pryputniewicz, D. R., Furlong, C. and Pryputniewicz, R. J., “ACES approach to the study of material properties of MEMS,” *Proc. Internat. Symp. on MEMS: Mechanics and Measurements*, Portland, OR, pp. 80-83, 2001.
10. Rosato, D. A., *Thermal analysis system: user’s manual*, Ver. 6.1, Harvard Thermal Inc., Harvard, MA, 2001.
11. SRAC, *COSMOS/M user’s guide*, Structural Research and Analysis Corporation, Santa Monica, CA, 1998.
12. Przekwas, A. J., Turowski, M., Furmanczyk, M., Hieke, A., and Pryputniewicz, R. J., “Multiphysics design and simulation environment for microelectromechanical systems,” *Proc. Internat. Symp. on MEMS: Mechanics and Measurements*, Portland, OR, pp. 84-89, 2001.
13. Pryputniewicz, R. J., *Engineering experimentation*, Worcester Polytechnic Institute, Worcester, MA, 1993.
14. Pryputniewicz, D. R., *ACES approach to the development of microcomponents*, MS Thesis, Worcester Polytechnic Institute, Worcester, MA, 1997.
15. Pryputniewicz, R. J., Galambos, P., Brown, G. C., Furlong, C., and Pryputniewicz, E. J., “ACES characterization of surface micromachined microfluidic devices,” *Internat. J. of Microelectronics and Electronic Packaging (IJMEP)*, 24(1):30-36, 2001.
16. Smith, J. H., “Micromachined sensor and actuator research at Sandia’s Microelectronics Development Laboratory,” *Sensors Expo ’96*, Anaheim, CA, pp.119-123, 1996.
17. Smith, J. H., Montague, S., Sniegowski, J. J., Murray, J., and McWhorter, P. J., “Embedded micromechanical devices for the monolithic integration of MEMS with CMOS,” *Proc. IEDM ’95*, pp. 609-615, 1995.
18. Rogers, M. S., and Sniegowski, J. J., “5-level polysilicon surface micromachine technology: application to complex mechanical systems,” *Proc. Solid State Sensor and Actuator Workshop*, Hilton Head, SC, 1998.
19. Pryputniewicz, R. J., “Hybrid approach to deformation analysis,” *Photonics*, Bellingham, WA, pp. 282-296, 1994.
20. Pryputniewicz, E. J., Miller, S. L., deBoer, M. P., Biederman, R. R., and Pryputniewicz, R. J., ”Hybrid approach to study of dynamic effects in MEMS microengines,” *Proc. IMAPS 27th Annual Symp*., Boxborough, MA, pp. 273-275, 2000.
21. Pryputniewicz, R. J., “Progress in microelectromechanical systems,” *Strain*, 43:13-25, 2007.
22. Pryputniewicz, R. J., Furlong, C., and Pryputniewicz, E. J., “Optimization of contact dynamics for an RF MEMS switch,” *Paper No. IMECE2002-39508*, ASME - Am. Soc. Mech. Eng., New York, NY, 2002.
23. Furlong, C., and Pryputniewicz, R. J., “Integrated approach to development of microelectronic contacts,” *Paper No. IPACK2007-33345*, ASME – Am. Soc. Mech. Eng., New York, NY, 2007.
24. Pryputniewicz, R. J., “Thermal management in RF MEMS Ohmic switches,” *Paper No. IPACK2007-33502*, ASME – Am. Soc. Mech. Eng., New York, NY, 2007.
25. Pryputniewicz, R. J., Pryputniewicz, D. R., and Pryputniewicz, E. J., “Effect of process parameters on TED-based Q-factor of MEMS,” *Paper No. IPACK2007-33094*, ASME – Am. Soc. Mech. Eng., New York, NY, 2007.
26. Zunino, J., and Skelton, D., “Department of Defense need for a microelectromechanical systems (MEMS) Reliability Assessment Program,” *Proc. Conf. on Reliability, Packaging, Testing, and Characterization of MEMS/MOEMS IV*, SPIE-5716:122–130, San Jose, CA, 2005.
27. Zunino, J. L. III, Skelton, D. R., Han, W., and Pryputniewicz, R. J., ”Hybrid approach to MEMS reliability assessment,” *Paper No. SPIE6563-03, Proc. Internat. Symp., on MOEMS-MEMS 2007: Reliability, Packaging, and Characterization of MEMS*, San Jose, CA, 2007.
28. Pryputniewicz, E.J., *ACES approach to the study of electrostatically driven MEMS microengines*, MS Thesis, Worcester Polytechnic Institute, Worcester, MA, 2000.
29. Pryputniewicz, R. J., Marinis, R. T., Klempner, A. R., and Hefti, P., “MEMS dynamics: measurements and modeling,” *Proc. 7th Internat. Symp. on MEMS and Nanotechnology* (*7th-ISMAN*), St. Louis, MO, pp. 167-181, 2006.
30. CFDRC, CFD-ACE+ *Multiphysics software*, http://www.cfdrc.com, 2006.
31. Przekwas, A. J., Turowski, M., Furmanczyk, M., Hieke, A., and Pryputniewicz, R. J., “Multiphysics design and simulation environment for microelectromechanical systems,” *Proc. Internat. Symp. on MEMS: Mechanics and Measurements*, Portland, OR, pp. 84-89, 2001.
32. Pryputniewicz, R. J., Wilkerson, P. W., Przekwas, A. J., and Furlong, C., “RF MEMS: modeling and simulation of switch dynamics,” *Proc. 35th Internat. Symp. on Microelectronics*, Denver, CO, pp. 267-272, 2002.

33. Furlong, C., *Hybrid, experimental and computational, approach for the efficient study and optimization of mechanical and electro-mechanical components*, Ph.D. Dissertation, Worcester Polytechnic Institute, Worcester, MA, 1999.
34. Brown, G. C., *Laser interferometric methodologies for characterizing static and dynamic behavior of MEMS*, Ph.D. Dissertation, Worcester Polytechnic Institute, Worcester, MA, 1999.
35. Pryputniewicz, R. J., "Quantitative determination of displacements and strains from holograms," Ch. 3 in *Holographic interferometry*, Vol. 68 of Springer Series in Sciences, Springer-Verlag, Berlin, pp. 33-72, 1995.
36. Pryputniewicz, R. J., "High precision hologrammetry," *Internat. Arch. Photogramm.*, 24:377-386, 1981.
37. Pryputniewicz, E. J., Miller, S. L., deBoer, M. P., Brown, G. C., Biederman, R. R., and Pryputniewicz, R. J., "Experimental and analytical characterization of dynamic effects in electrostatic microengines," *Proc. Internat. Symp. on Microscale Systems*, Orlando, FL, pp. 80-83, 2000.
38. Pryputniewicz, R. J., Marinis, T. F., Soucy, J. W., and Furlong, C., "Development of packaging for MEMS inertial sensors," *Proc. IEEE-PLANS2004*, Monterey, CA, pp. 56-62, 2004.
39. Pryputniewicz, R. J., "Hologram interferometry from silver halide to silicon and … beyond," *Proc. SPIE*, 2545:405-427, 1995.
40. Brown, C., and Pryputniewicz, R. J., "Holographic microscope for measuring displacements of vibrating microbeams using time-average electro-optic holography," *Opt. Eng.*, 37:1398-1405, 1998.
41. Klempner, A. R., Hefti, P., Marinis, R. T., and Pryputniewicz, R. J., "Development of a high stability optoelectronic laser interferometric microscope for characterization and optimization of MEMS," *Proc. 15th Internat. Invitational UACEM Symp*., Springfield, MA, pp. 275-285, 2004.
42. Marinis, T. F., Soucy, J. W., Hanson, D. S., Pryputniewicz, R. J., Marinis, R. T., and Klempner, A. R., "Isolation of MEMS devices from package stresses by use of compliant metal interposers," *Proc. 56th IEEE Electronic Components & Technology Conf. (56th-IEEE-ECTC)*, paper No. P1S25-MEMS, San Diego, CA, 2006.
43. Pryputniewicz, R. J., Tan, X. G., and Przekwas, A. J., "Modeling and measurements of MEMS. gyroscopes," *Proc. IEEE-PLANS2004*, Monterey, CA, pp. 111-119, 2004.
44. Mihailovich, R. E., Kim, M., Hacker, J. B. H., Sovero, A., Studer, J., Higgins, J. A., and DeNatale, J. F., "MEM relay for reconfigurable RF circuits," *IEEE Microwave Wireless Components Lett*., 11:53-55, 2001.

MEMS reliability assessment: Preliminary results. Article. Jan 2007.Â This paper describes the methodology and discusses preliminary results that have been obtained relating measurements that facilitate MEMS reliability assessment (MRA) on representative samples used. Regardless of their application, the MEMS have to be reliable while in use. MEMS reliability, however, is application specific and, usually, has to be developed on a case by case basis. The results presented herein were obtained, using a recently developed optoelectronic laser interferometric microscope (OELIM) methodology, in a planned program on MEMS reliability assessment. The presentation is il